Youcef Mammeri*

A reaction-diffusion system to better comprehend the unlockdown: Application of SEIR-type model with diffusion to the spatial spread of COVID-19 in France

Abstract: We wondered that if a reaction-diffusion model considering only the mean daily movement of susceptible, exposed and asymptomatic individuals was enough to describe the spread of the COVID-19 virus. The model was calibrated using data on the confirmed infection and death from France as well as their initial spatial distribution. First, the system of partial differential equations is studied, then the basic reproduction number, $\mathcal{R}_0$ is derived. Second, numerical simulations, based on a combination of level-set and finite differences, shown the spatial spread of COVID-19 from March 16 to June 16. Finally, scenarios of unlockdown are compared according to variation of distancing, or partially spatial lockdown.

1 Introduction

A disease outbreak, called Coronavirus Disease 2019 or COVID-19 in brief, emerged in the city of Wuhan late 2019 [19]. COVID-19 belongs to the *Coronaviridae* family. A family of coronaviruses that cause diseases in humans, and COVID-19 may cause severe infection, that can be lethal [10, 3]. COVID-19 spreads fast. According to WHO [20], only 67 days from the beginning of the outbreak in China last December 2019 were necessary to infect the first 100,000 people worldwide. It is observed that the virus moves from East to West. Beginning in China, it is, at the time of writing, in America after crossing Europe.

Last 30th of January, WHO characterized COVID-19 as Public Health Emergency of International Concern (PHEI) and urge countries to put in place strong measures to detect disease early, isolate and treat cases, trace contacts, and promote social distancing measures commensurate with the risk [21]. In response, the world implemented its actions to reduce the spread of the virus. Limitations on mobility, social distancing, and self-quarantine have been applied. More than 100 countries established full or partial lockdown. All these efforts have been made to reduce the transmission rate of the virus. For the time being, COVID-19 infection is still on the rise.

Many mathematical models have been proposed to help governments as an early warning device about the size of the outbreak, how quickly it will spread, and how effective control measures may be. Most of the models are (discrete or continuous) SIR-type and few are taken into account the spatial spread. [7] implemented a metapopulation network model described by a discrete-time Susceptible-Exposed-Infected-Recovered (SEIR) compartmental model. The model gives an estimate of the expected number of cases in mainland China at the end of January 2020, as well as the global distribution of infected travelers. [22] fused

*Corresponding Author: Youcef Mammeri:** Laboratoire Amiénois de Mathématique Fondamentale et Appliquée, CNRS UMR 7352, Université de Picardie Jules Verne, 80069 Amiens, France, E-mail: youcef.mammeri@u-picardie.fr

an SEIR metapopulation model to simulate epidemic. [5] incorporated daily movements in an SEIR model, while [8] proposed a statistical model to handle the diffusion of covid-19 in Italy.

Here, spatial propagation is translated by a diffusion and the reaction terms are deduced from an extension from the classical SEIR model by adding a compartment of asymptomatic infected [1]. We aim at predicting the spread of COVID-19 by giving maps the basic reproductive numbers $\mathcal{R}_0$ and its effective reproductive number $\mathcal{R}_{\text{eff}}$. Do a reaction-diffusion model, which consider only the mean daily movement of susceptible, exposed and asymptomatic individuals, describe correctly the spread of the COVID-19 virus? Afterward, we also assess possible scenarios of unlockdown.

The rest of the paper is organized as follows. Section 2, outlines our methodology. Here the model was explained, where the data was taken, and its parameter estimates. Section 3 contained the qualitative analysis for the model. Here, we provide the reproductive number $\mathcal{R}_0$, then compare strategies to handle unlockdown. Finally, section 4 outlines our brief discussion on some measures to limit the outbreak.

2 Materials and methods

2.1 Confirmed and death data

In this study, we used the publicly available dataset of COVID-19 provided by the Santé Publique France. This dataset includes daily count of confirmed infected cases, recovered cases, hospitalizations and deaths. Data can be downloaded from https://www.data.gouv.fr/fr/datasets/donnees-hospitalieres-relatives-a-lepidemie-de-covid-19/. These data are collected by the National Health Agency and are directly reported public and unidentified patient data, so ethical approval is not required. The map of population density are from Géoportail (https://www.geoportail.gouv.fr) established by the National Geographic Institute. Data concerning transport are extracted from National Institute of Statistics and Economic Studies (https://statistiques-locales.insee.fr/).
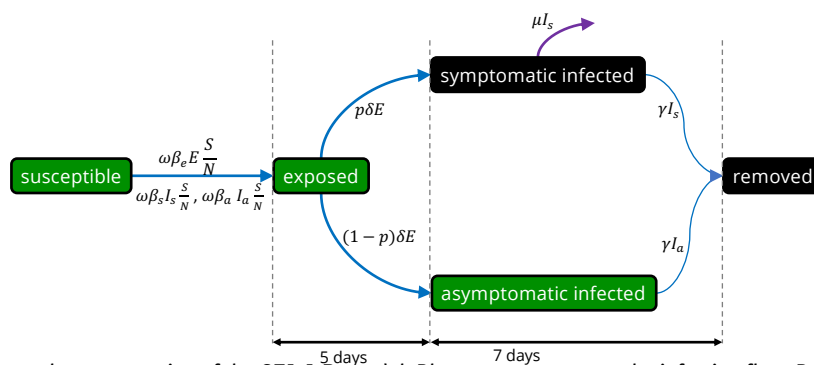
2.2 Mathematical model

Figure 1: Compartmental representation of the SEI_aI_sR-model. Blue arrows represent the infection flow. Purple arrows denote the death. Green compartments indicate moving individuals. Parameters are described in Table A of Figure 3 below. N is the total living population.

We focus our study on five components of the epidemic flow (Figure 1), *i.e.* the densities of Susceptible individual (S), Exposed individual (E), symptomatic Infected individual (I_s), asymptomatic Infected individual (I_a), and Removed individual (R). To simplify the readings, treatments are not distinguished between quarantine, hospitalization or medicine. To build the mathematical model, we followed the standard strategy developed in the literature concerning SIR model [6, 2, 1]. We assumed that susceptible can be infected by exposed and by infected individuals. We suppose that only susceptible, exposed and asymptotic individ-

uals are moving. The dynamics is governed by a system of three partial differential equations (PDE) and two ordinary differential equations (ODE) as follows, for $\mathbf{x} = (x, y) \in \Omega \subset \mathbb{R}^2$, $t > 0$,

$$
\begin{cases}
\partial_t S - d(t)\Delta S = -\omega(t)\left(\beta_e E + \beta_s I_s + \beta_a I_a\right)\dfrac{S}{N} \\[2mm]
\partial_t E - d(t)\Delta E = \omega(t)\left(\beta_e E + \beta_s I_s + \beta_a I_a\right)\dfrac{S}{N} - \delta E \\[2mm]
\partial_t I_a - d(t)\Delta I_a = (1-p)\delta E - \gamma I_a \\[2mm]
\qquad\quad I_s' = p\delta E - (\gamma + \mu)I_s \\[2mm]
\qquad\quad R' = \gamma(I_a + I_s).
\end{cases}
\tag{1}
$$

Frontiers being now closed during the pandemic, homogeneous Neumann boundary conditions is imposed. The total living population is $N = S + E + I_a + I_s + R$ and the death is $D' = \mu I_s$. No new recruit is added. The parameters are described in Table A of Figure 3.

2.3 Parameters estimation

Latency period and infection period have been estimated as 5 days and 7 days respectively [11], and thus $\delta = 1/5, \gamma = 1/7$. To account for the lockdown and unlockdown, the average number of contacts is updated as follows [12]

$$
\omega(t) = \begin{cases}
\omega_0 \text{ if } t \le t_{bol} \\[2mm]
\omega_0 e^{-\rho_l(t-t_{bol})} \text{ if } t_{bol} \le t \le t_{eol} \\[2mm]
\dfrac{(1-\eta)\omega_0}{1 + ((1-\eta)e^{\rho_l(t_{eol}-t_{bol})} - 1)e^{-\rho_u(t-t_{eol})}} \text{ if } t \ge t_{eol},
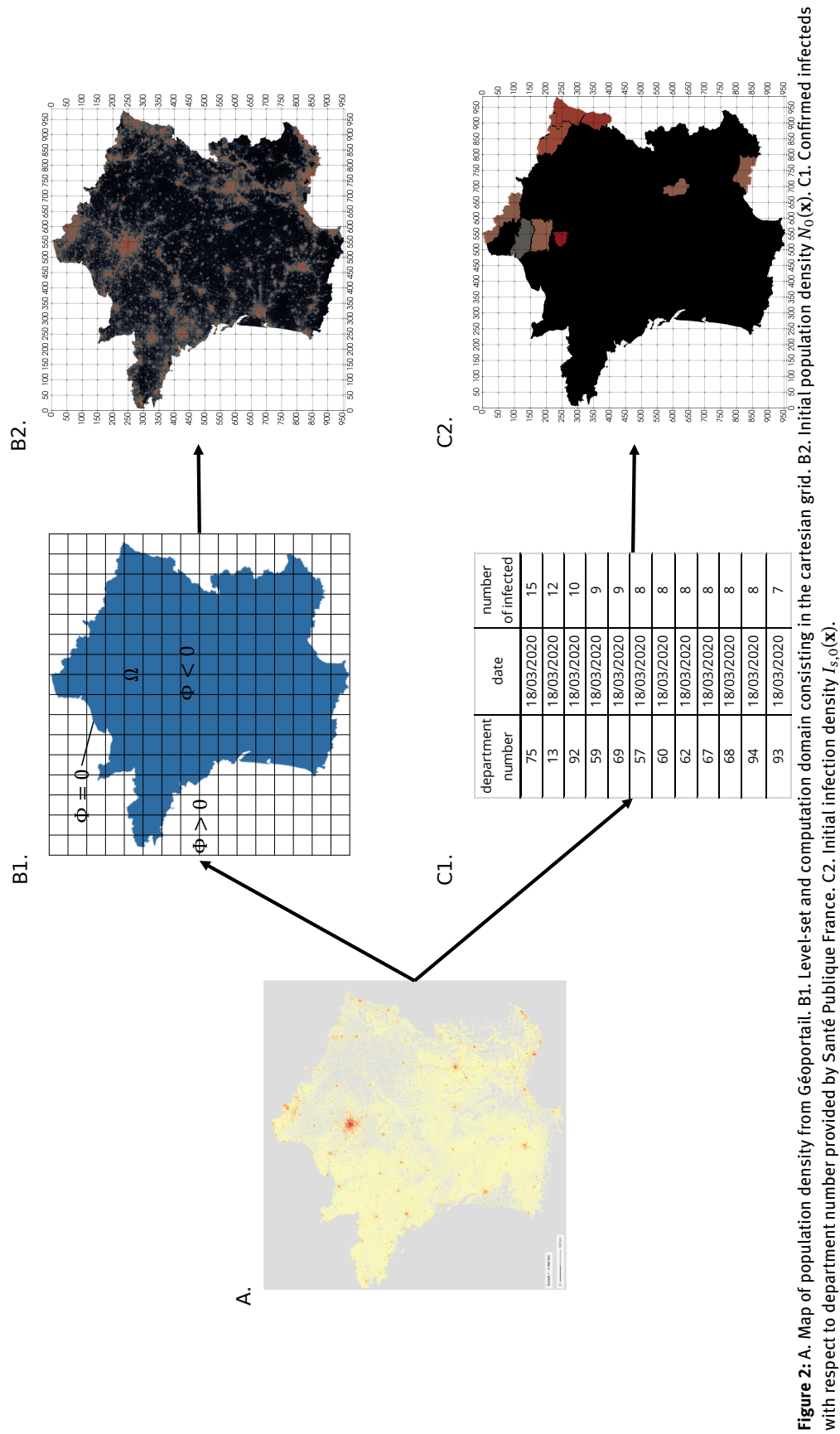\end{cases}
\tag{2}
$$

while the diffusion coefficient is set up to

$$
d(t) = \begin{cases}
d_0 \text{ if } t \le t_{bol} \\[2mm]
d_0 e^{-\rho_l(t-t_{bol})} \text{ if } t_{bol} \le t \le t_{eol} \\[2mm]
\dfrac{d_0}{1 + (e^{\rho_l(t_{eol}-t_{bol})} - 1)e^{-\rho_u(t-t_{eol})}} \text{ if } t \ge t_{eol}.
\end{cases}
\tag{3}
$$

Here *bol* denotes for beginning of lockdown and *eol* for end of lockdown. The parameter $0 \le \eta \le 1$ is a varying coefficient translating respect for distancing. Note that ω_0 is the average number of contacts before any intervention and is supposed to be constant. From INSEE, the daily commuting in France is around $25 km$, the value of d_0 is fixed equal to $\frac{25^2}{16}$ [13, 17]. Eight parameters $(\omega_0, \rho_l, \rho_u, \beta_e, \beta_s, \beta_a, p, \mu)$ remain to be determined. Nevertheless, $\omega_0, \beta_e, \beta_s, \beta_a$ are not independently identifiable and the identification problem reduces to the seven parameters $\theta = (\rho_l, \rho_u, \omega_0\beta_e, \omega_0\beta_s, \omega_0\beta_a, p, \mu)$. Given, for n days, the observations $I_{s,obs}(t_i)$ and $D_{obs}(t_i)$, the cost function consists of the nonlinear least square function

$$
J(\theta) = \sum_{i=1}^n \left(I_{s,obs}(t_i) - \overline{I_s}(t_i, \theta)\right)^2 + (D_{obs}(t_i) - \overline{D}(t_i, \theta))^2,
$$

with constraints $\theta \ge 0$. Here $\overline{I_s}(t_i, \theta) = \int_\Omega I_s(\mathbf{x}, t_i, \theta)d\mathbf{x}$ and $\overline{D}(t_i, \theta) = \int_\Omega D(\mathbf{x}, t_i, \theta)d\mathbf{x}$ denote the output of the mathematical model at time t_i computed with the parameters θ. The optimization problem is solved using Approximate Bayesian Computation combined with a quasi-Newton method [4].

Figure 2: A. Map of population density from Géoportail. B1. Level-set and computation domain consisting in the cartesian grid. B2. Initial population density $N_0(\mathbf{x})$. C1. Confirmed infecteds with respect to department number provided by Santé Publique France. C2. Initial infection density $I_{s,0}(\mathbf{x})$.

department number	date	number of infected
75	18/03/2020	15
13	18/03/2020	12
92	18/03/2020	10
59	18/03/2020	9
69	18/03/2020	9
57	18/03/2020	8
60	18/03/2020	8
62	18/03/2020	8
67	18/03/2020	8
68	18/03/2020	8
94	18/03/2020	8
93	18/03/2020	7

2.4 Numerical discretization

From the map of the country, the level-set [14, 16] is defined as the function ϕ such that the territory

$$\Omega := \left\{ \mathbf{x} \in \mathbb{R}^2; \ \phi(\mathbf{x}) < 0 \right\},$$

and its boundary is the zero level of ϕ The exterior normal is $\vec{n} = \frac{\nabla\phi}{||\nabla\phi||}$. The computation domain consists in a cartesian grid given by the image pixels (Figure 2). Then the map of population density allows to build initial population density $N_0(\mathbf{x})$. From data of confirmed infecteds, the spatial distribution of initial infection $I_{s,0}(\mathbf{x})$ with respect to department number is created (Figure 2).

Finally, Runge-Kutta 4 is used for the time discretization and central finite difference for the space discretization.

3 Results

3.1 Global well-posedness and basic reproduction numbers

Let us suppose that for all time, $d_1 \leq d(t) \leq d_0$. We first prove that the model is globally well posed.

Theorem 3.1. *Let* $0 \leq S_0, E_0, I_{a,0}, I_{s,0}, R_0 \leq N_0$ *be the initial datum. Then there exists a unique global in time weak solution* $(S, E, I_a, I_s, R) \in L^\infty(\mathbb{R}_+, L^\infty(\Omega))^5$, *of the initial boundary value problem. Moreover, the solution is nonnegative and* $S + E + I_a + I_s + R \leq N_0$.

Proof. Let $Y = (S, E, I_a, I_s, R)$. Thanks to the comparison principle and according to the Duhamel formulation, we look for a time $T > 0$ such that the map

$$
\begin{aligned}
\Phi(Y) \quad := \quad \Bigg(& \mathcal{G}_d \star S_0 - \int\limits_0^t \mathcal{G}_d \star \left(\omega \left(\beta_e E + \beta_s I_s + \beta_a I_a \right) \frac{S}{N} \right) ds, \\[2mm]
& \mathcal{K}_e \star E_0 + \int\limits_0^t \mathcal{K}_e \star \left(\omega \left(\beta_e E + \beta_s I_s + \beta_a I_a \right) \frac{S}{N} \right) ds, \\[2mm]
& \mathcal{K}_s \star I_{a,0} + (1-p)\delta \int\limits_0^t \mathcal{K}_s \star E \, ds, \\[2mm]
& e^{-(\gamma+\mu)t} I_0 + p\delta \int\limits_0^t e^{-(\gamma+\mu)(t-s)} E \, ds, \\[2mm]
& R_0 + \gamma \int\limits_0^t I_s + I_a \, ds \Bigg)
\end{aligned}
$$

is a contraction mapping from the closed ball

$$
\left\{ Y = (S, E, I_a, I_s, R) \in L^\infty(\mathbb{R}_+, L^\infty(\Omega))^5; \ \sup_{t\in[0,T]} ||Y(t, .) - Y_0||_{L^\infty(\Omega)} < +\infty \right\}
$$

onto itself. Here $\mathcal{G}_d$, $\mathcal{K}_e$, and $\mathcal{K}_s$ are the kernels of the respective operators $\partial_t - d\Delta$, $\partial_t - d\Delta + \delta$, and $\partial_t - d\Delta + \gamma$ for $d = d_0$ or d_1. According to [15], there exists a constant $C_\Omega > 0$ depending only on Ω such that the kernels satisfy

$$||\mathcal{G}_d(t, .)||_{L^1(\Omega)} \leq C_\Omega, ||\mathcal{K}_e(t, .)||_{L^1(\Omega)} \leq C_\Omega, ||\mathcal{K}_s(t, .)||_{L^1(\Omega)} \leq C_\Omega.$$

Combining with the fact that the integral terms of the right-hand-side are locally Lipschitz, choosing $T \ll \frac{1}{C_\Omega}$ allows to apply Picard's fixed point theorem [9].

If $f = (f_1, \ldots, f_5)$ denotes the right-hand-side of the system (1), and $Y = (S, E, I_a, I_s, R)$, since $f_i(Y_i = 0) \geq 0$, we deduce that the solution is nonnegative if the initial datum is nonnegative. Finally, maximum principle provides boundedness of solution. □

We give a condition on parameters such that the disease has an exponential initial growth.

Theorem 3.2. *Let $(S_0, E_0, I_{a,0}, I_{s,0}, 0)$ be a nonnegative initial datum. If the basic reproduction number*

$$\mathcal{R}_0 := \omega_0 \left(\frac{\beta_e}{\delta} + \frac{(1-p)\beta_a}{\gamma} + \frac{p\beta_s}{\gamma + \mu} \right) \frac{S_0}{N_0} > 1,$$

then (E, I_a, I_s) exponentially grows.

This number has an epidemiological meaning. The term $\frac{\beta_e}{\delta}$ represents the transmission rate by exposed during the average latency period $1/\delta$. The term $\frac{(1-p)\beta_a}{\gamma}$ is the transmission rate by asymptomatic during the average infection period $1/\gamma$, and the last one is the part of symptomatic.

Proof. A linearization around $(S_0, E_0, I_{a,0}, I_{s,0}, 0)$ is written as the linear system of differential equations

$$\begin{pmatrix} E \\ I_a \\ I_s \end{pmatrix}' (t) = \begin{pmatrix} d_0\Delta + \omega_0\beta_e \frac{S_0}{N_0} - \delta & \omega\beta_a \frac{S_0}{N_0} & \omega\beta_s \frac{S_0}{N_0} \\ (1-p)\delta & d_0\Delta - \gamma & 0 \\ p\delta & 0 & -(\gamma + \mu) \end{pmatrix} \begin{pmatrix} E \\ I_a \\ I_s \end{pmatrix}.$$

Let $(v_k)_{k \geq 1}$ be an orthonormal basis of eigenfunctions of the Laplace operator with the homogeneous Neumann boundary condition, *i.e.* $-\Delta v_k = k^2 v_k$. Therefore, the characteristic polynomial of the matrix

$$\begin{pmatrix} -d_0 k^2 + \omega_0\beta_e \frac{S_0}{N_0} - \delta & \omega\beta_a \frac{S_0}{N_0} & \omega\beta_s \frac{S_0}{N_0} \\ (1-p)\delta & -d_0 k^2 - \gamma & 0 \\ p\delta & 0 & -(\gamma + \mu) \end{pmatrix},$$

is $P(x) = x^3 + a_2 x^2 + a_1 x + a_0$, with $a_0 = (\gamma + \mu)(d_0 k^2 + \gamma)(d_0 k^2 + \delta)(1 - \mathcal{R}_k)$ and

$$\mathcal{R}_k := \omega_0 \left(\frac{\beta_e}{d_0 k^2 + \delta} + \frac{(1-p)\beta_a}{d_0 k^2 + \gamma} + \frac{p\beta_s}{\gamma + \mu} \right) \frac{S_0}{N_0}.$$

If $\mathcal{R}_k > 1$, there is at least one positive eigenvalue that coincides with an initial exponential growth rate of solutions. □

To reflect the spatiotemporal dynamic of the disease, we consider the effective reproduction number

$$\mathcal{R}_{\text{eff}}(\mathbf{x}, t) := \omega(t) \left(\frac{\beta_e}{\delta} + \frac{(1-p)\beta_a}{\gamma} + \frac{p\beta_s}{\gamma + \mu} \right) \frac{S(\mathbf{x}, t)}{N(\mathbf{x}, t)},$$

and its mean with respect to the domain Ω

$$\overline{\mathcal{R}_{\text{eff}}}(t) := \frac{1}{\mathcal{A}(\Omega)} \int_\Omega \mathcal{R}_{\text{eff}}(\mathbf{x}, t) d\mathbf{x}.$$

The value of $\mathcal{R}_0$ is computed in Table A of Figure 3.

We now establish the asymptotic behavior of solution.

Theorem 3.3. *With the same assumptions as Theorem 3.1. Suppose moreover $\omega_0\beta_e \leq \delta$. Then the solution converges almost everywhere to the Disease Free Equilibrium $(S^\star, 0, 0, 0, R^\star)$ with $S^\star + R^\star = N^\star$.*

Proof. From the last differential equation in system (1), we deduce that R is an increasing function bounded by $N(0)$. Thus $R(t)$ converges to $R^\star$ a.e. as t goes to $+\infty$. Then integrating over time this equation provides

$$R(\mathbf{x}, t) - R(\mathbf{x}, 0) = \gamma \int_0^t I_a(\mathbf{x}, s) + I_s(\mathbf{x}, s)\, ds$$

and

$$R^\star(\mathbf{x}) - R_0(\mathbf{x}) = \gamma \int_0^{+\infty} I_a(\mathbf{x}, s) + I_s(\mathbf{x}, s)\, ds,$$

which is finite. Furthermore, I_s, I_a also go to 0 a.e. as $t \to +\infty$ thanks to the positivity of the solution. Multiplying the second equation by E and integrating over Ω give

$$\frac{1}{2}\frac{d}{dt}\int_\Omega E^2(\mathbf{x}, t)d\mathbf{x} + d\int_\Omega (\nabla E)^2(\mathbf{x}, t)d\mathbf{x} = \int_\Omega \omega\,(\beta_s I_s + \beta_a I_a)\frac{S}{N}E + (\omega\beta_e\frac{S}{N} - \delta)E^2.$$

Since $0 \le \frac{S}{N} \le 1$ and $\omega \le \omega_0$, Young's inequality followed by Poincaré inequality provide

$$\frac{1}{2}\frac{d}{dt}\int_\Omega E^2(\mathbf{x}, t)d\mathbf{x} + dC_\Omega\int_\Omega E^2(\mathbf{x}, t)d\mathbf{x} \le \int_\Omega \frac{\omega_0^2\beta_s^2}{2\varepsilon}I_s^2 + \frac{\omega_0^2\beta_a^2}{2\varepsilon}I_a^2 + (\frac{\varepsilon}{2} + \omega_0\beta_e - \delta)E^2.$$

Since I_s and I_a go to 0 when $t \to +\infty$, it is enough to choose $\varepsilon > 0$ such that $dC_\Omega + \delta - \omega_0\beta_e - \frac{\varepsilon}{2} > 0$, to conclude that $E \to 0$ a.e. $\qquad\square$

Remark 3.4. *The basic reproduction number $\mathcal{R}_0$ can be computed thanks to the next generation matrix of the model without diffusion as in [18]. Since the infected individuals are in E, I_a and I_s, new infections ($\mathcal{F}$) and transitions between compartments ($\mathcal{V}$) can be rewritten as*

$$\mathcal{F} = \begin{pmatrix} \omega(\beta_e E + \beta_s I_s + \beta_a I_a)\frac{S}{N} \\ 0 \\ 0 \end{pmatrix}, \quad \mathcal{V} = \begin{pmatrix} \delta_e E \\ \gamma I_a - (1 - p)\delta E \\ (\gamma + \mu)I_s - p\delta E \end{pmatrix}.$$

Thus, $\mathcal{R}_0 = \rho(FV^{-1})$ of the next generation matrix

$$FV^{-1} = \begin{pmatrix} \frac{\omega\beta_e S_0}{\delta N_0} + \frac{\omega(1-p)\beta_a S_0}{\gamma N_0} + \frac{\omega p\beta_s S_0}{(\gamma+\mu)N_0} & \frac{\omega\beta_a S_0}{\gamma N_0} & \frac{\omega\beta_s S_0}{(\gamma+\mu)N_0} \\ 0 & 0 & 0 \\ 0 & 0 & 0 \end{pmatrix}.$$

3.2 Model resolution

Calibration of the model is done from January 24, 2020, the day of first confirmed infection, to June 8, 2020. Since $\mathcal{R}_0 = 3.425257$ and $1 - \frac{1}{\mathcal{R}_0} = 0.708051$, 70% of the population is set as susceptible to the infection due to the herd immunity. The objective function J is computed to provide a relative error of order less than 10^{-2}. In Figure 3, Table A shows estimated parameters. Remark that $\omega_0\beta_e \le \delta$. The rest of the Figure compares the data and the fitted total symptomatic infected and death of the posterior distribution.
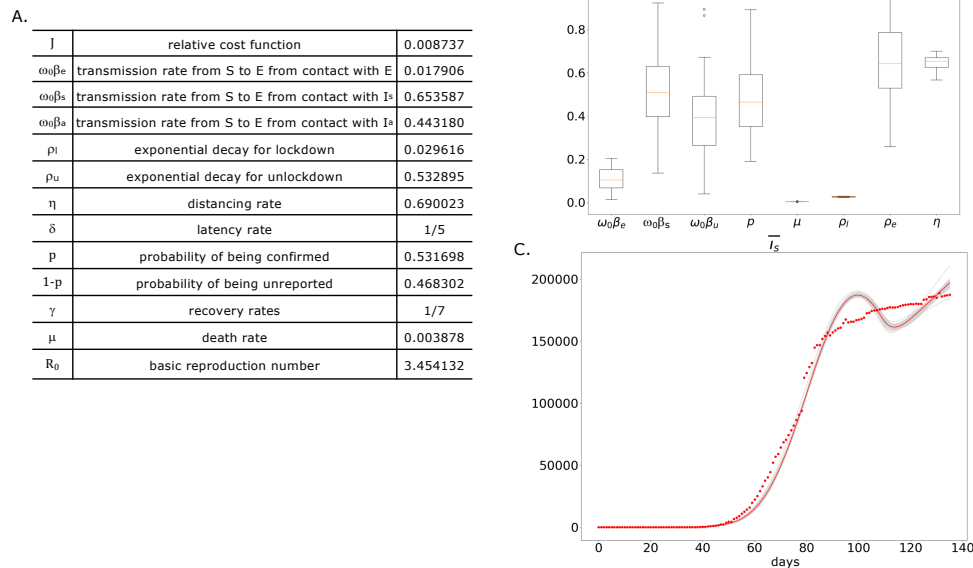
A.

J	relative cost function	0.008737
$\omega_0\beta_e$	transmission rate from S to E from contact with E	0.017906
$\omega_0\beta_s$	transmission rate from S to E from contact with I_s	0.653587
$\omega_0\beta_a$	transmission rate from S to E from contact with I_a	0.443180
ρ_l	exponential decay for lockdown	0.029616
ρ_u	exponential decay for unlockdown	0.532895
η	distancing rate	0.690023
δ	latency rate	1/5
p	probability of being confirmed	0.531698
1-p	probability of being unreported	0.468302
γ	recovery rates	1/7
μ	death rate	0.003878
R_0	basic reproduction number	3.454132

Figure 3: A. Parameters calibrated according to data from Santé Publique France. B. Boxplot of the posterior distribution computed from these data. C. Fitted total symptomatic infected of the posterior distribution in grey , median in red straight line, mean is dotted line.

3.3 Spatial spread of covid-19

Simulations are performed from January 24, 2020, the day of first confirmed infection, to June 16. Images are 957×984 pixels, time step is chosen to verify the stability condition preserving positivity, and $\eta = 0.65$.

Figure 4-A presents the day before lockdown, the disease is mainly located in regions North (Hauts-de-France, Île-de-France), East (Grand Est), Center-East (Rhône) and South-East (Bouches-du-Rhône). When lockdown ends on May 10, Figure 4-B1 shows that the disease remains located into these regions, except for the South where it almost vanishes. Provided that distancing is predominantly respected (here $\eta = 0.65$), the density of symptomatic infecteds is decreasing until June 16 everywhere (Figure 4-B2). The model reproduces spatial propagation as evidenced by the unlockdown maps proposed by the French government (https://solidarites-sante.gouv.fr/soins-et-maladies/maladies/maladies-infectieuses/coronavirus/etat-des-lieux-et-actualites/article/indicateurs-de-l-activite-epidemique).

New data and maps are available (https://www.gouvernement.fr/info-coronavirus/carte-et-donnees). For example, the new hospitalizations on June 16, 2020 further confirms that the model provides a realistic representation of the epidemic.

Figures 4-C represents what would happen if nothing has been done. On May 10, the disease is located in the same regions, but with a greater number of infected. As a consequence, the spread continues from East to West. While the disease vanishes in the Eastern part of the country on June 16, the West is peaking. It is important to see that, without intervention, the total number of infected is high and the whole country is deeply affected.
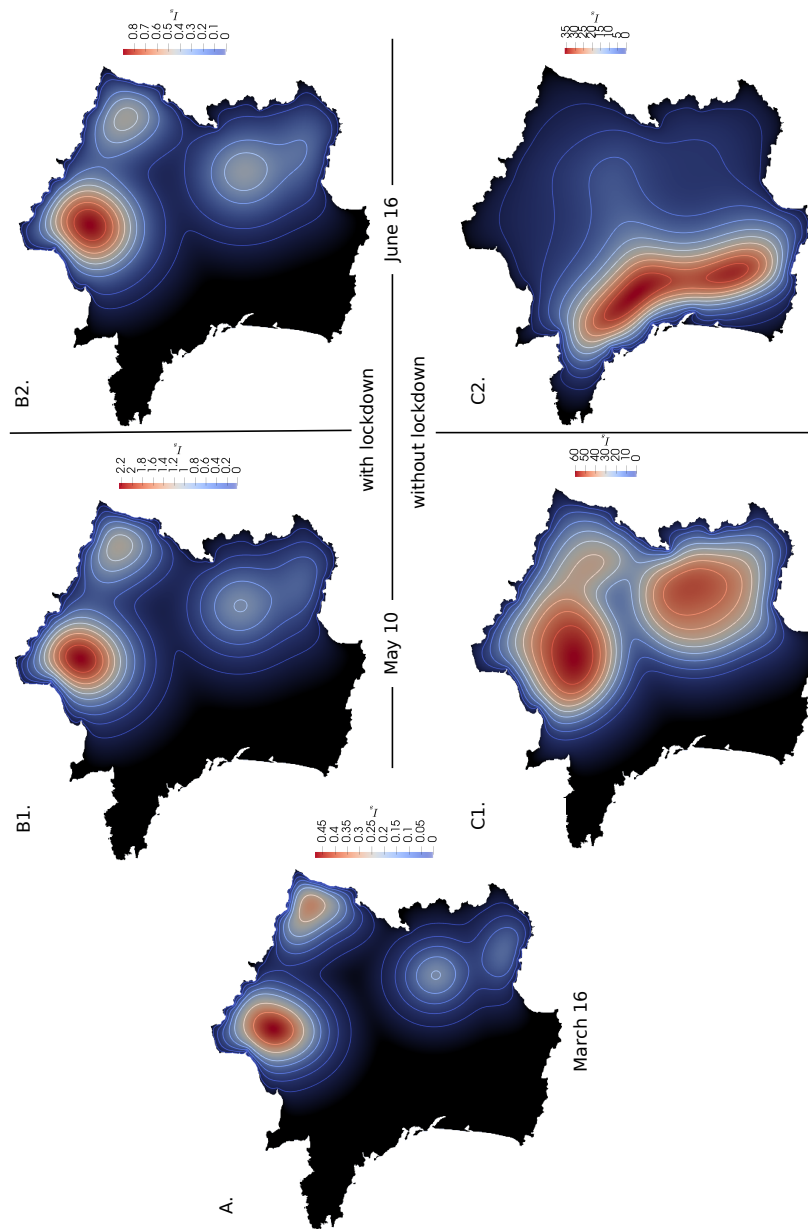
Figure 4: A. Spatial distribution of symptomatic infected density on March 16, one day before lockdown. B. Spatial distribution of symptomatic infected density on May 10 (B1), one day before unlockdown, and on June 16 (B2) assuming that no lockdown has been done.

3.4 Strategies for unlockdown

A naive strategy is to unlock the regions where $\mathcal{R}_{\text{eff}}(\mathbf{x}, .)$ is the lowest. Looking at the maps in Figures 5, we see that the effective reproduction number before the lockdown is between 3.34 and 3.42 (Figures 5-A). On May 10, it goes down and is between 0.38 and 0.42 (Figures 5-B). After May 10, with a distancing mostly respected ($\eta = 0.65$), $\mathcal{R}_{\text{eff}}(\mathbf{x}, .)$ increases again. It exceeds 1 with lower value (1.04) in the regions that have been most affected upstream (Figures 5-C).

Figure 5: Spatial distribution of effective reproduction number one day before lockdown March 16 (A), one day before unlockdown May 10 (B), and on June 16 (C).

A less forced strategy is to believe in the respect of distancing after lockdown. With this set of parameters, $\overline{\mathcal{R}_{\text{eff}}}$ remains lower than 1 if $\eta \geq 0.68$. As shown in Figure 6-A, provided that at least 68% of the individuals respect the distancing rules, the number of symptomatic infected individuals is controlled. Figure 6-B shows that in this case, the effective reproduction number $\overline{\mathcal{R}_{\text{eff}}}$ remains less than 1. Below 68% regarding distancing, the number of symptomatic infected increases again and $\overline{\mathcal{R}_{\text{eff}}}$ becomes greater than 1.

A third strategy, more constraining for some, is to continue the lockdown in the most affected areas. Here, lockdown is continued on the eastern half, while the western half is free. Then the number of symptomatic infected and the effective reproduction number pursue their decay as shown in Figure 6 (dotted lines). It is important to note that in the simulation no individuals move from a confined to an unconfined region. A homogeneous Neumann condition, equal to 0, is imposed along this fictitious frontier.
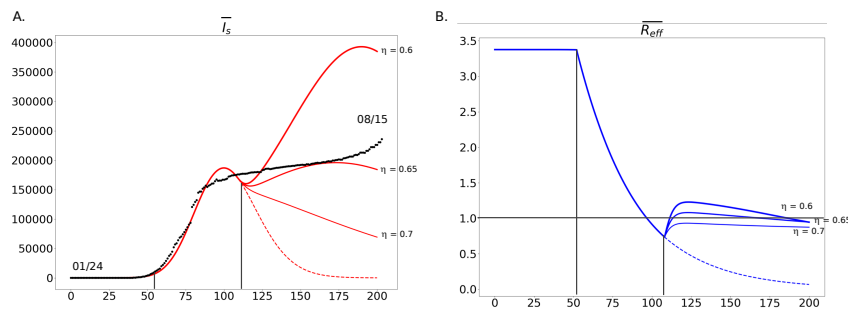

Figure 6: A. Total number of symptomatic infected with $\eta = 0.6, 0.65, 0.7$ (——) and with lockdown on East region (- - -). B. Mean effective reproduction number with $\eta = 0.6, 0.65, 0.7$ (——) and with lockdown on East region (- - -). Lockdown started on March 17 and ended on May 11. Dots denote for the confirmed data.

4 Discussion

Lockdown has reduced both the number of infections and the spread. The propagation focused in the Eastern half and kept the West intact. Without lockdown, the whole country would be affected and more severely. Lockdown caused a significant reduction of the reproduction number, from 3.42 to 0.38. Since the number of susceptible individuals remain large, as soon as contacts increase, the effective reproduction number $\mathcal{R}_{\text{eff}}$ grows and can exceed 1.

With a lack of treatment, social distancing remains the most effective means. We notice that it has to be highly respected (here at over 68%). As shown in Figure 6-A, the number of symptomatic infected individuals, therefore potentially hospitalized, is restrained as soon as at least 63% of the individuals respect the distancing, Nevertheless, this constraint can be relaxed since it can be imposed only in the most infectious areas.

In summary, to obtain a possible unlockdown map, the local value of the effective reproduction number should be taken into account, as well as the number of infected individuals and the direction of the spread of the disease.

Although this is a simplified model based only the population density and mean daily commuting, it reproduces the dynamic of the disease accurately. It is an indication that the covid is a contact disease and therefore population density is an essential source of transmission.

For example, the model could be improved by considering a larger diffusion along major axes of travel (*i.e.* $d = d(\mathbf{x}, t)$), by taking local effects of distancing (*e.g* $\eta = \eta(\mathbf{x}, t)$ where $\eta(\mathbf{x}, t) = 0$ in closed schools), or by opening of the frontiers (by changing the boundary conditions and adding new recruits).

References

[1] J. Arcede, R. Caga-anan, C. Q. Mentuda, and Y. Mammeri. Accounting for symptomatic and asymptomatic in a seir-type model of covid-19. *Math. Model. Nat. Phenom.*, 15(34), 2020. URL https://doi.org/10.1051/mmnp/2020021.

[2] F. Brauer and C. Castillo-Chavez. *Mathematical Models in Population Biology and Epidemiology*. Springer, New York, NY, 2012. URL https://doi.org/10.1007/978-1-4614-1686-9.

[3] N. Chen, M. Zhou, X. Dong, J. Qu, F. Gong, Y. Han, Y. Qiu, J. Wang, Y. Liu, Y. Wei, J. Xia, T. Yu, X. Zhang, and L. Zhang. Epidemiological and clinical characteristics of 99 cases of 2019 novel coronavirus pneumonia in wuhan, china: A descriptive study. *The Lancet*, 395(10223):507–513, 2020. URL https://doi.org/10.1016/S0140-6736(20)30211-7.

[4] K. Csilléry, M. G. Blum, O. E. Gaggiotti, and O. François. Approximate bayesian computation (abc) in practice. *Trends in ecology & evolution*, 25(7):410–418, 2010. URL https://doi.org/10.1016/j.tree.2010.04.001.

[5] L. Danon, E. Brooks-Pollock, M. Bailey, and M. Keeling. A spatial model of covid-19 transmission in england and wales: early spread and peak timing. *medRxiv*, 2020. URL https://www.medrxiv.org/content/early/2020/02/14/2020.02.12.20022566.

[6] O. Diekmann and J. Heesterbeek. *Mathematical Epidemiology of Infectious Diseases: Model Building, Analysis and Interpretation*. Chichester: John Wiley, 2000. URL https://doi.org/10.1093/ije/30.1.186.

[7] L. Gardner. Modeling the spreading risk of 2019-ncov. 31 january 2020. retrieved 25 march 2020. Technical report, Center for Systems Science and Engineering, Johns Hopkins University, 2020. URL https://systems.jhu.edu/research/public-health/ncov-model-2.

[8] D. Giuliani, M. Dickson, G. Espa, and F. Santi. Modelling and predicting the spatio-temporal spread of coronavirus disease 2019 (covid-19) in italy. *arXiv*, 2020. URL https://arxiv.org/abs/2003.06664.

[9] D. Henry. *Geometric theory of semilinear parabolic equations*. Springer, 1981.

[10] D. S. Hui, E. I. Azhar, T. A. Madani, F. Ntoumi, R. Kock, O. Dar, G. Ippolito, T. D. Mchugh, Z. A. Memish, C. Drosten, A. Zumla, and E. Petersen. The continuing 2019-ncov epidemic threat of novel coronaviruses to global health - the latest 2019 novel coronavirus outbreak in wuhan, china. *International Journal of Infectious Diseases*, 91:264–266, 2020. URL https://doi.org/10.1016/j.ijid.2020.01.009.

[11] S. A. Lauer, K. Grantz, Q. Bi, F. K. Jones, Q. Zheng, H. R. Meredith, A. S. Azman, N. G. Reich, and J. Lessler. The incubation period of coronavirus disease 2019 (covid-19) from publicly reported confirmed cases: Estimation and application. *Annals of Internal Medicine*, 03 2020. URL https://doi.org/10.7326/M20-0504.

[12] Z. Liu, P. Magal, O. Seydi, and G. Webb. Predicting the cumulative number of cases for the covid-19 epidemic in china from early data. *Mathematical Biosciences and Engineering*, 17(mbe-17-04-172):3040, 2020. URL http://dx.doi.org/10.3934/mbe.2020172.

[13] A. Okubo. *Diffusion and Ecological Problems: Mathematical Models*. Springer-Verlag, Berlin- Heidelberg-New York, 1980.

[14] S. Osher and R. Fedkiw. *Level Set Methods and Dynamic Implicit Surfaces*. Springer New York, 2002.

[15] E. Ouhabaz. *Analysis of Heat Equations on Domains*. London Math. Soc. Monographs Series, Princeton University Press, 2005.

[16] J. Sethian. *Level Set Methods and Fast Marching Methods: Evolving Interfaces in Computational Geometry, Fluid Mechanics, Computer Vision, and Materials Science*. Cambridge University Press, 1999.

[17] N. Shigesada and K. Kawasaki. *Biological Invasions: Theory and Practice*. Oxford University Press, 1997.

[18] P. van den Driessche and J. Watmough. Reproduction numbers and sub-threshold endemic equilibria for compartmental models of disease transmission. *Mathematical Biosciences*, 180(1-2):29–48, 2000. URL https://doi.org/10.1016/S0025-5564(02)00108-6.

[19] *Naming the coronavirus disease (COVID-19) and the virus that causes it*. World Health Organization, Accessed March 21, 2020 2020. URL https://www.who.int/emergencies/diseases/novel-coronavirus-2019/technical-guidance/naming-the-coronavirus-disease-(covid-2019)-and-the-virus-that-causes-it.

[20] *COVID-19*. World Health Organization, Accessed March 25, 2020 2020. URL https://www.who.int/docs/default-source/coronaviruse/transcripts/who-transcript-emergencies-coronavirus-press-conference-full-13mar2020848c48d2065143bd8d07a1647c863d6b.pdf?sfvrsn=23dd0b04_2.

[21] *Statement on the Second Meeting of the International Health Regulations. (2005). Emergency Committee Regarding the Outbreak of Novel Coronavirus (2019-nCoV)*. World Health Organization, 2020. URL https://www.who.int/news-room/detail/30-01-2020-statementon-the-second-meeting-of-the-international-health-regulations-(2005)-emergency-committee-regarding-the-outbreak-of-novel-coronavirus-(2019-ncov).

[22] J. T. Wu, K. Leung, and G. M. Leung. Nowcasting and forecasting the potential domestic and international spread of the 2019-ncov outbreak originating in wuhan, china: A modelling study. *The Lancet*, 395(10225):689–697, 2020. URL https://doi.org/10.1016/S0140-6736(20)30260-9.